Shallow Slow Earthquake Episodes Near the Trench Axis Off Costa Rica

Satoru Baba[1], Kazushige Obara[1], Shunsuke Takemura[1], Akiko Takeo[1], and Geoffrey A. Abers[2]

[1]Earthquake Research Institute, The University of Tokyo, Tokyo, Japan

[2]Department of Earth and Atmospheric Sciences, Cornell University, Ithaca, New York, United States of America

Corresponding author: Satoru Baba (babasatoru@eri.u-tokyo.ac.jp)

Key Points:

- Shallow very low frequency earthquakes (VLFEs) and tremors are detected off Costa Rica near the Middle America Trench
- Distribution of VLFEs and tremors is spatially correlated with slow slip events
- Scaled energy of shallow slow earthquakes off Costa Rica is 10^{-9}–10^{-8}, which is similar to those in Nankai

Abstract

Slow earthquakes are mainly distributed in regions surrounding seismogenic zones along the plate boundaries of subduction zones. In the Central American subduction zone, large regular interplate earthquakes with magnitudes of 7–8 occur repeatedly around the Nicoya Peninsula, in Costa Rica, and a tsunami earthquake occurred off Nicaragua, just north of Costa Rica, in 1992. To clarify the spatial distribution of various slip behaviors at the plate boundary, we detected and located very low frequency earthquakes (VLFEs) around the Nicoya Peninsula using a grid-search matched-filter technique with synthetic templates based on a regional three-dimensional model. VLFEs were active in September 2004 and August 2005, mainly near the trench axis, updip of the seismogenic zone. The distribution of VLFEs overlaps with large slip areas of slow slip events. Low frequency tremor signals were also found in high-frequency seismogram envelopes within the same time windows as detected VLFEs; thus, we also investigated the energy rates of tremors accompanied by VLFEs. The range of scaled energy, which is the ratio of the seismic energy rate of a tremor to the seismic moment rate of accompanying VLFE and related to the rupture process of seismic phenomena, was 10^{-9}–10^{-8}. The along-dip separation of shallow slow and large earthquakes and the range of the scaled energy off Costa Rica are similar to those in shallow slow earthquakes in Nankai, which shares a similar thermal structure along the shallow plate boundary.

Plain language summary

Slow earthquakes generally occur on the plate boundaries of subduction zones. We detected and located very low frequency earthquakes (VLFEs), which are a type of slow earthquake, off Costa Rica. The VLFEs occurred at a depth range of 6–10 km, and their spatial distribution is correlated with slow slip events, another type of slow earthquakes. The spatial separation of slow and large regular earthquakes is common to the Nankai subduction zone. Low frequency tremor signals, which are also classified as slow earthquakes, are also found in seismograms at higher frequencies within the same time windows of detected VLFEs. We also estimated the ratio of energy rates of tremors to moment rates of VLFEs, which relates to the rupture process of seismic phenomena. The ratio is 10^{-9}–10^{-8} off Costa Rica, similar to that in shallow slow earthquakes in the Nankai subduction zone.

1. Introduction

Slow earthquakes are mainly observed in regions surrounding seismogenic zones, which are the areas that rupture in large regular earthquakes, along the plate boundaries of subduction zones (e.g., Obara & Kato, 2016) or strike-slip faults (e.g., Nadeau & Dolenc, 2005; Wang & Barbot, 2020). Various types of slow earthquakes, such as low frequency tremors (tectonic tremors; e.g., Obara, 2002), low frequency earthquakes (LFEs; e.g., Shelly et al., 2006), very low frequency earthquakes (VLFEs; e.g., Obara & Ito, 2005), and slow slip events (SSEs; e.g., Dragert et al., 2001) have been observed in many subduction zones. Although there are areas where some types of slow earthquakes are not spatiotemporally correspondent (Hutchison, 2020; Hutchison & Ghosh, 2016, 2019), they often correlate spatiotemporally, which is termed episodic tremor and slip (ETS). ETSs were observed in deep Cascadia (e.g., Ghosh et al., 2015; Rogers & Dragert, 2003) and deep Nankai (e.g., Ito et al., 2007; Obara, 2011), for example. Recently, in the Nankai subduction zone, pore fluid pressure changes have been observed during tremor and VLFE activities and are considered to reflect shallow SSEs by offshore borehole observations (Araki et

al., 2017; Nakano et al., 2018). The hypocenters and focal mechanisms of slow earthquakes are generally consistent with shear slip on the plate boundaries. VLFE episodes and SSEs occur in almost identical source regions and their temporal changes of moment release are similar during an ETS, therefore VLFE episodes are considered as proxies for SSEs (Hutchison & Ghosh, 2019; Ito et al., 2007; Nakano et al., 2018; Yokota & Ishikawa, 2020). In summary, the distribution of slow earthquakes is related to large earthquake slip areas, interplate coupling, or fluid distribution (e.g., Baba et al., 2020b; Ghosh et al., 2015; Obara & Kato, 2016).

In the Central American subduction zone, the Cocos plate subducts beneath the Caribbean plate at the Middle America Trench at a rate of approximately 80 mm/year (Figure 1b; referred from NUVEL1A; DeMets et al., 1994). In this subduction zone, large thrust-type earthquakes with a moment magnitude (M_W) of 7–8 occur with a recurrence interval of tens of years around the Nicoya Peninsula, in Costa Rica (light blue areas in Figure 1a; Protti, 1995; Yue et al., 2013). The coseismic slip areas of these large earthquakes are distributed at a depth range of 10–35 km beneath the peninsula and off the coast. The latest large earthquake with M_W of 7.6 occurred on 5 September, 2012 (green contour lines in Figure 1a; Yue et al., 2013). In the vicinity, a tsunami earthquake with M_W of 7.6 also occurred off Nicaragua, just north of Costa Rica, on 2 September, 1992 (dark blue area in Figure 1a; Satake, 1994).

In addition to large regular and tsunami earthquakes, slow earthquakes also occur around the Nicoya Peninsula. The Global Navigation Satellite System data revealed that SSEs with M_W of 6.6–7.2 occur at intervals of 21.7±2.6 months (Jiang et al., 2012; Xie et al., 2020). The large slip area of the SSE in 2007 was separated into downdip and updip areas by the seismogenic slip area (Jiang et al., 2012, 2017; Outerbridge et al., 2010). The spatiotemporal change in relation to the 2012 M_W 7.6 earthquake was investigated by previous studies (Dixon et al., 2014; Voss et al., 2017), and an SSE preceded the 2012 M_W 7.6 earthquake (Voss et al., 2018) in the almost same area of the 2007 SSE, similar to both the slow slip before the 2011 Tohoku earthquake in Japan (Ito et al., 2013; Kato et al., 2012) and the slow slip before the 2014 Iquique earthquake in Chile (Kato & Nakagawa, 2014; Ruiz et al., 2017).

By using high-frequency (>1 Hz) seismograms, Brown et al. (2009) and Outerbridge et al. (2010) located LFEs and tremors in 2007, respectively (Figure 1a). The tremors and LFEs were located in almost the same area, downdip of the seismogenic zone. Although tremors and LFEs were temporally correlated with the SSE, the location of tremors and LFEs were separated from the large slip area of the 2007 SSE. On the other hand, Walter et al. (2011) located many tremors in the offshore region from 2007 to 2009. Walter et al. (2013) also found that VLFEs appeared in seismograms in a frequency range of 0.02–0.05 Hz and were temporally correlated with tremors in the time period of the 2008 SSE. Based on beamforming analysis, they estimated the propagation direction and the propagation speed of VLFE signals and suggested that VLFEs also occurred in offshore areas. Due to the limitations of a conventional analysis, however, epicenters of VLFEs in offshore areas were not located. Therefore, the detailed spatial distribution of VLFEs off Costa Rica is still not well understood.

The spatial variation of slow and large regular earthquakes can reflect the spatial heterogeneity of the frictional conditions on the plate boundary (e.g., Baba et al., 2020b). To clarify the spatial relationship between slow and large regular earthquake distribution around the Nicoya Peninsula, an accurate spatial distribution of VLFEs is needed. Thus, we detected VLFEs around the Nicoya Peninsula using a temporary broadband seismic network from August 2004 to January 2006 because signals of VLFEs are less attenuated than those of tremors and propagate longer

distances. The method is based on the matched-filter technique. Template waveforms from possible VLFE locations were evaluated by numerical simulations of seismic wave propagation using a regional three-dimensional (3D) velocity structure model. In addition, scaled energy is an informative parameter for the rupture process of seismic phenomena (Kanamori & Rivera, 2006). Although scaled energies of slow earthquakes around Japan were well investigated by previous studies (e.g., Ide & Yabe, 2014; Yabe et al., 2019; 2021), those in Costa Rica was not estimated. Therefore, we also estimated the seismic energy rate functions of tremors accompanied by VLFEs by using high frequency (2–8 Hz) seismograms to evaluate the scaled energy of slow earthquakes around the Nicoya Peninsula.

2. VLFE analysis

2.1. Data and method

2.1.1. Data

We used waveforms of a temporary seismic network, Tomography Under Costa Rica and Nicaragua (TUCAN; Abers & Fischer, 2003), recorded from August 2004 to January 2006. There were 49 broadband seismic stations in four lines (Figure 1b). For the VLFE analysis, we used 14 stations near the Nicoya Peninsula in Costa Rica (shown in Figure 1a), because signals of VLFEs are relatively clear in these 14 stations and using all stations causes higher computational cost for synthetic calculations. After removing instrumental responses, the seismograms for VLFE detection were resampled at one sample per second. We applied a bandpass filter in the frequency range of 0.02–0.05 Hz (e.g., Ghosh et al., 2015; Ito et al., 2009; Takemura et al., 2019), because this frequency band is less affected by microseismic noises (e.g., Hasselmann, 1963; Kaneko et al., 2018). We verified that the large amplitude surface waves are generally matched well between observed and synthetic waveforms in a higher frequency range (Figure S1; 0.02-0.06 Hz).

2.1.2. Matched-filter technique

The detection procedure used for VLFEs is similar to that used in our previous study (Baba et al., 2020a). The horizontal-component seismograms of many stations were noisy; therefore, it is difficult to use horizontal-component seismograms for the location of VLFEs (Figure S2). Thus, we used only the vertical-component seismograms for the VLFE analysis although it is usual to analyze VLFEs by using three-component seismograms. We placed 175 virtual source grids on the Cocos Plate boundary at a uniform interval of 0.1° (Figure 2a) and computed synthetic waveforms from these source grids to the stations in Costa Rica using an open-source seismic wave propagation code (OpenSWPC; Maeda et al., 2017). We used a three-dimensional velocity structure model constructed by combining CRUST 1.0 (Laske et al., 2013), Slab2 (Hayes et al., 2018), and ETOPO1 (Amante & Eakins, 2009), setting the minimum *S*-wave velocity in the solid columns to 1.0 km/s. We adopted the values of a mean oceanic slab structure (Christensen & Salisbury, 1975) for the physical parameters of the subducting slab (Table S1). For the physical parameters of the other layers except for the slab, we used the values of CRUST 1.0, and the default parameter set of OpenSWPC. The cross-section of the structure model is shown in Figure S3. The model covered the region enclosed by the red line (Figure 1b), which was discretized by a uniform grid interval of 0.2 km. The assumed VLFE moment rate function was a Küpper wavelet with a source duration of 15 s and an M_W of 4.0 (Figure 4 of Maeda et al., 2017). Since focal mechanisms of VLFEs are consistent with shear slip on the plate boundaries in previous studies (Cascadia: Ghosh et al., 2015; Nankai: Ito et al., 2009; Nakano et al., 2018; Sugioka et al., 2012; Takemura et al., 2019), the focal mechanism at each source grid was assumed to be consistent with the

geometry of the plate boundary of Slab2 and the plate motion model, NUVEL-1A (DeMets et al., 1994). The time window of each template was set to 150 s from the event origin time. Hereafter, we simply refer to these synthetic waveforms as template waveforms. Examples of template waveforms at updip and downdip source grids are shown in Figures 2b and 2c, respectively. The signal first arrives at MANS and the variation of amplitudes is small for the updip source, whereas signals first arriving at FINA exhibit amplitudes in or near the Nicoya Peninsula that are much larger than in other areas for the downdip source.

We then calculated cross-correlation coefficients (CCs) between the filtered template waveforms and observed seismograms every 1 s. We selected events with station-averaged coefficients larger than a threshold defined as 9.5 times the median absolute deviation (MAD) of the distributions. In order to decrease false detections by non-VLFE signals on the condition that only the vertical-component seismograms can be used and the station coverage along the azimuth direction is poor, we adopted a strict detection threshold compared to previous studies (e.g., 8 × MAD in Shelly et al., 2007, and Baba et al., 2018 and 9 × MAD in Baba et al., 2020a). The changes of CCs when focal mechanisms or depths of assumed source models are different from the geometry of the plate boundary are shown in Figure S4.

2.1.3. VLFE location and discarding false detections

Although a strict detection threshold was employed, there are false detections that are caused by other signals, such as local or regional regular earthquakes or teleseismic events. To exclude local or regional earthquakes, we compared the origin time of detected events with a catalog of local and regional regular earthquakes constructed by El Observatorio Vulcanológico y Sismológico de Costa Rica, Universidad Nacional (Catálogo de Temblores de Costa Rica, 2004-2006; Protti, personal comm.). We discarded events whose epicentral distances were less than 150 km and origin times were within ±50 s from the local or regional earthquakes listed in this earthquake catalog. To discard false detections by teleseismic events, we removed the events detected between the *P*-wave arrivals and 600 s after *S*-wave arrivals of teleseismic events ($M_W \geq 5$) in the catalog of the United States Geological Survey. The event amplitudes and CCs are positively correlated in general, but events with high amplitudes and low average CCs occasionally appear. These events are considered to be false detections due to teleseismic events absent in the catalogs. Therefore, we did not count events with average CCs below 0.56 and relative amplitudes to templates higher than 0.4 (Baba et al., 2018; 2020a). If the amplitude relative to the template with M_W of 4.0 was smaller than 0.05, we did not count the event because the signal was too small to judge whether the event is truly existed or not.

For the remaining events, we calculated the variance reduction (VR) between the template and observed waveforms. We estimated VRs using only the vertical-component seismograms of relatively quiet stations in and around the Nicoya Peninsula (MANS, CABA, FINA, CRUP, and PALM), because amplitude differences between updip and downdip events are large in these stations:

$$VR = \left[1 - \frac{\sum_i \int \{f_i(t) - c g_i(t)\}^2 dt}{\sum_i \int \{f_i(t)\}^2 dt}\right] \times 100\% , \quad (1)$$

where $f_i(t)$ and $g_i(t)$ are the observed and template waveforms at the i-th station, respectively, and c is the relative amplitude of the observed waveform to the template. We selected events whose VRs were larger than 30%. This threshold is set by trial and error based on visual identifications of VLFEs in the observed data.

After the above procedures, falsely detected events still remained because we only used the vertical-component seismograms, and the array configuration was cross shaped. To discard the remaining false detections, we estimated the normalized-and-stacked amplitude, azimuth, and velocity of signal propagation by applying delay-and-sum beamforming (Section 3.1 of Rost & Thomas, 2002; Walter et al., 2013) to vertical-component seismograms. After normalizing the waveform of each station by its maximum amplitude in the 150 s time window, we searched for the azimuth and velocity that maximized the stacked amplitude by performing a grid search for the azimuth between 135–315º with 1º intervals and the velocity between 2–5 km/s with 0.1 km/s intervals. We first used the along-strike stations in both Costa Rica and Nicaragua (brown inverted triangles in Figure 1b) to discard teleseismic events. The amplitudes of Costa Rican VLFEs at the Nicaraguan stations are generally very small compared with those in the Costa Rican stations due to geometrical spreading, but amplitudes for teleseismic events are similar. Therefore, we selected events whose stacked normalized amplitude normalized by the number of stations was smaller than 0.6 because events with large stacked signals are suspected to be teleseismic earthquakes (Figure S5). We then conducted another beamforming analysis for the remaining events using the same stations as the matched-filter analysis, and selected events whose azimuth was 200–230º. Finally, to avoid duplicate detection, only one event was counted every 60 s from the remaining VLFE candidates. We only counted the event whose averaged CC was the highest spatiotemporally.

2.1.4. Estimation of the moments of events

We estimated the source durations of detected VLFEs by comparing template waveforms with source durations of 10–50 s with observed waveforms (e.g., Yabe et al., 2021). The M_W of the templates was set to be 4.0. The source duration that resulted in the highest values of CC between the observed and template waveforms was adopted.

We also calculated the amplitude of an event relative to the template waveforms using the same method as Baba et al. (2020b). The relative amplitude can be used to calculate the seismic moment of each VLFE. The seismic moment rate of a VLFE was calculated by dividing its seismic moment by its source duration. To evaluate the estimation error of moment rates of VLFEs, we calculated moment rates by assuming the various source durations whose CCs between synthetic and observed waveforms are more than 90% of the maximum CC. Although there are errors in the order of 0.2, we verified that the order of moment rates does not change (Figure S6).

2.2. Results

We detected 68 VLFEs during the analysis period. Example traces of a VLFE located at 85.8°W and 9.4°N are shown in Figure3. The signal of this VLFE first arrives at MANS and propagates to inland stations (top panel of Figure 3). This feature was successfully modeled for the updip templates (Fig. 2b). There is a tremor signal in the frequency range of 2–8 Hz in the same time window (middle and bottom panels of Figure 3). The cumulative number of VLFEs showed significant increases in September 2004 and August 2005 (Figure 4a). In August 2005, an SSE was reported by Jiang et al. (2012); therefore, SSE and VLFE activities were temporally correlated. The M_W and source duration of VLFEs in Costa Rica were mainly distributed in 3.4–4.2 and 10–30 s, respectively (Figures 5a, b). The M_W and source duration of VLFEs have a positive correlation (Figure 5c) like shallow VLFEs in Nankai, Japan (Sugioka et al., 2012; Takemura et al., 2019). The relationship between durations and magnitudes of VLFEs and SSEs

(Jiang et al., 2012; Voss et al., 2017) in Costa Rica is closer to the range inferred from the scaling law of slow earthquakes than that of regular earthquakes by Ide et al. (2007) (Figure 5c).

Most of the VLFEs (62 events) are distributed where the plate boundary is at a depth range of 6–10 km below the sea level, near the trench axis off the Nicoya Peninsula (Figure 4b), at the updip of the seismogenic zone. The distribution of these VLFEs is consistent with the VLFEs in 2008 suggested by Walter et al. (2013). When locating some events using both vertical and horizontal-component seismograms whose signal to noise (SN) ratios are relatively high for the verification of the analysis by using vertical-component seismograms only, the high CC areas overlap and the epicenters were also located near the trench axis, although there are differences of 0.1–0.2º (Figure S2). The area overlaps with the shallower part of the large slip area of the 2007 SSE (Jiang et al., 2017) or summed SSE slip in 2007–2012 (Dixon et al., 2014). Although the slip distribution of the 2005 SSE was not estimated in previous studies, our results suggest that the 2005 SSE can also have a large slip area near the trench axis, similar to the 2007 SSE. The distribution of VLFEs lies within the gap between large slip areas of thrust-type large interplate earthquakes with an M_W of 7–8 around the Nicoya Peninsula and the 1992 tsunami earthquake with an M_W of 7.6. The distribution of VLFEs also separated from the afterslip area of the 2012 M_W 7.6 earthquake (Malservisi et al., 2015).

The distribution of the CC shows the resolution of the location of VLFEs. By the distribution of CC, it is confirmed that most of the VLFEs were located near the trench axis. CCs for more than half of the events exceeded the threshold only for updip templates (Figure 6a). For several events, CCs exceeded the threshold both updip and downdip of the seismogenic zone with a larger CC in the updip region. The area where CCs are more than 90% of the maximum CC is concentrated only in the updip area (Figure 6b). On the other hand, 6 VLFEs were located at a depth of ~40 km at the downdip of large earthquakes (Figure 4b). Although focal mechanisms may not be thrust-type and the areas where CCs are larger than the threshold are widely distributed, we verified that regular earthquakes listed in the earthquake catalog by El Observatorio Vulcanológico y Sismológico de Costa Rica in the updip and downdip areas are located in the updip and downdip areas respectively by this method (Figure S7). However, we cannot exclude the possibility that such VLFEs occur in the updip region in real because, in such cases, bimodal CC distributions tend to appear both in the updip and downdip (Figure 6c). Of course, there is a possibility that such VLFEs really occur in the downdip region because the locations of such VLFEs were near the locations of previously reported LFEs (Brown et al. 2009) and tremors (Outerbridge et al. 2010). In this study, the SN ratios of VLFEs detected in the downdip region are very low; hence, it is difficult to judge whether such VLFEs occur in downdip or updip, because it is hard to judge which station the signal of the VLFE arrival first due to the similar arrival times at updip stations. The reason for the small number and the low SN ratio of downdip events may be that slow earthquakes in the downdip region were inactive during 1.5 years of the temporary array. To investigate whether deep VLFEs really exist, an analysis with a longer dataset is needed in future work.

3. Estimations of seismic energy rates for tremors accompanied by VLFEs

3.1. Data and method

Tremor signals were also found in the frequency range of 2–8 Hz within the time windows of detected VLFEs (middle panel of Figure 3; Figure S8). It is difficult to locate tremors in the offshore region by using an onshore network because sources of tremors are distant from the network and signals of tremors attenuate strongly compared to VLFE (0.02–0.05 Hz) signals.

Based on the spatiotemporal correlation between VLFEs and tremors reported in other regions (e.g., Ghosh et al., 2015; Maeda & Obara, 2009; Tamaribuchi et al., 2019) and the interpretation that VLFEs and tremors are components of broadband slow earthquake phenomena (Gomberg et al., 2016; Hawthorne & Bartlow, 2018; Ide & Maury, 2018), we estimated the energy rate functions of tremors accompanied by VLFEs by assuming that a tremor occurs at the same location as the VLFE, i.e., the VLFE source grid with the highest CC as written in Section 2.1.3 (e.g., Yabe et al., 2021). We simulated the waveforms at the location of a VLFE using the same model which is described in Section 2.1.2 but discretized by a finer grid interval (0.04 km). The simulated envelope shapes are different from observed ones due to a simple pulse source time function (details in the caption of Figure S9), but the arrival times of maximum *S*-wave amplitudes in the frequency range of 2–8 Hz are consistent with observed tremor waveforms (Figure S9). The interval of source grids for the VLFE detection was set as 0.1°, therefore, we supposed that a VLFE and the corresponding tremor occurred at the same location in the order of 10 km.

We also used waveforms of the TUCAN network similarly to the VLFE detection. After applying a bandpass filter of 2–8 Hz, the envelope waveforms were calculated by taking the root-mean-square of sums of three-component squared seismograms and a smoothing time window of 3 s (bottom panel of Figure 3). The envelope waveforms were resampled at one sample per second.

3.1.1. Quality factor of the apparent *S*-wave attenuation

To estimate the energy rate functions of tremors accurately, we estimated the quality factor of the apparent *S*-wave attenuation ($Q_{app.}$), based on the coda-normalization method (e.g., Aki, 1980; Yoshimoto et al., 1993). First, we selected some isolated regular earthquakes (Figure S10). To eliminate the effect of differences in source size and site amplification, observed maximum *S*-wave amplitudes were normalized by averaged coda amplitudes within a lapse time of 80-90 s. The coda-normalized maximum *S*-wave amplitude of the *i*-th earthquake at the *j*-th station (A_{ij}) and the distance between the hypocenter of the *i*-th earthquake and *j*-th station (L_{ij}) have the following relationship (Takemura et al., 2017):

$$\ln\left(L_{ij}A_{ij}\right) = -\frac{\pi f_c Q_{app.}^{-1}}{V_s} L_{ij} + C' , \quad (2)$$

where V_s is the *S*-wave velocity (assuming 3.5 km/s in this study; Maeda & Obara, 2009; Yabe et al., 2019; 2021), f_c is the central frequency (assuming 5 Hz in this study), and *C'* is a constant. By solving Equation (2) by the least-squares method, we estimated $Q_{app.}^{-1}$ as $10^{-2.42}$ (Figure 7a).

3.1.2. Site amplification factor

We estimated the site amplification factor at 2–8 Hz using relative coda amplitudes (e.g., Maeda and Obara, 2009). Coda amplitudes at a certain time window generally depend on the source size and site amplification (e.g., Chapters 2 and 3 of Sato et al., 2012). Therefore, the ratio of the coda wave amplitude at a station to that at a reference station for the same event depends only on the site amplification factor relative to a reference station.

We calculated the ratios of the coda amplitudes for each station to those of MANS (reference station) for each regular earthquake used in Section 3.1. The time window for evaluating relative coda amplitudes is the same as that in coda-normalization in Section 3.1. Then we calculated the average of the coda amplitude ratios of all earthquakes for each station. The estimated relative site amplification factors at each station used in the estimations of the energy rate functions of tremors are shown in Figure 7b. We compared coda amplitudes of regular

earthquakes at MANS with those at the JTS, a permanent station of the Global Seismograph Network by Incorporated Research Institutions for Seismology and International Deployment of Accelerometers (Scripps Institution of Oceanography, 1986). The average ratio of coda amplitudes at MANS to those at JTS is 1.14, suggesting that the condition of MANS site is very similar to that of the JTS.

3.1.3. Seismic energy rate of tremors

By using apparent attenuation ($Q_{app.}^{-1}$) and site amplification in the previous subsections, we estimated the energy rate functions of tremors. The source energy rate function of a tremor ($E_j\ (t)$) using the amplitude of the *j*-th station is calculated by the following formula (Maeda & Obara, 2009):

$$E_j(t) = 2\pi V_S r_j^2 \rho A'^2_j(\mathrm{t} + t_j)\exp\left(2\pi f_c Q_{app.}^{-1} t_j\right), \quad (3)$$

where $A'_j\ (t)$ is the site-corrected amplitude of the envelope waveform of the *j*-th station, r_j is the hypocentral distance from the accompanying VLFE, t_j is the travel time from the VLFE source, and ρ is the density (assuming 2,700 kg/m^3). For calculating $E_j\ (t)$, we used a 180 s time window that started 60 s before the origin time of VLFEs. We calculated the CCs of all station pairs in Figure 7b. The range of CCs of each pair is 0.5–0.85 for the event of Figure 3 (Figure S11). To estimate the source energy rate function of the tremor, we only used stations whose CCs with at least one other station exceeded 0.6.

The seismic energy rate W_j using the amplitude of the *j*-th station is given by the integration of the source energy rate function $E_j\ (t)$ in time:

$$W_j = \frac{1}{t_2 - t_1}\int_{t_1}^{t_2} E_j(t)dt, \quad (4)$$

where t_1 and t_2 are the start and end of the integration range, respectively. The integration range is defined as the period in which the values of $E_j\ (t)$ exceeded 20% of the maximum value of $E_j\ (t)$ (Figure 8). The seismic energy rate of a tremor (W_0) was obtained by calculating the average W_j of all stations. The error of W_0 was obtained by calculating the standard deviation of W_j.

3.2. Results

For 13 of 68 VLFEs, there were no station pairs whose CCs were larger than 0.6 when estimating the energy rates of accompanying tremors, because such tremors may not be detected by technical limitations or tremors and VLFEs may be distinct phenomena. We, therefore, estimated energy rates of 55 tremors. The energy rates of tremors were mainly distributed in 10^3–$10^{5.5}$ J/s (Figure 9). There is a positive correlation between the energy rates of tremors and the moment rates of the corresponding VLFEs. We estimated the scaled energy by calculating the ratio between the seismic energy rate of a tremor and the seismic moment rate of the corresponding VLFE. The scaled energy of slow earthquakes off Costa Rica is mainly distributed in the range of 10^{-9}–10^{-8} (dotted lines in Figure 9).

4. Discussion

4.1. Shallow ETS off Costa Rica

As shown in Figure 3 and Figure S8, VLFEs and tremors often were temporally correlated. The activation of VLFEs and tremors in August 2005 temporally correlates with the 2005 SSE reported by Jiang et al. (2012). VLFEs and tremors occurred mainly in the updip area in August

2005; hence, the slip area of the 2005 SSE can be distributed in the updip area near the trench axis, similar to the 2007 SSE. In areas where shallow VLFEs occurred, subseafloor hydrological observatories recorded pore fluid pressure transients in 2000 (Brown et al., 2005), 2003–2004 (Solomon et al., 2009), and 2007–2013 (Davis et al., 2011; 2015). They interpreted that pore fluid pressure transients were caused by SSEs. Spatial correspondence of pore fluid change in the periods of previous studies and VLFE activity in 2005 near the trench off Costa Rica suggests the occurrence of a shallow ETS, as with the Nankai subduction zone (Araki et al., 2017; Nakano et al., 2018).

4.2. Heterogeneity of the frictional property on the plate boundary

To discuss the heterogeneity of the frictional property on the plate boundary, we compare the differences of stress drops and interplate coupling between the VLFE area and the seismogenic zone in the Central American subduction zone. In this study, we showed that most of VLFEs were located at a depth range of 6–10 km on the plate boundary, which is updip of the seismogenic zone. The stress drop of VLFEs in the Nankai subduction zone was estimated to be 0.1–10 kPa (Ito & Obara, 2006), therefore we expect that the stress drop of VLFEs in Costa Rica is similar. This is much smaller than the stress drop of earthquakes in the tsunami earthquake rupture area (1.2 MPa; Bilek et al., 2016). In addition, the interplate coupling was estimated to be weak at a depth range of 6–10 km (Feng et al., 2012), and strong in the seismogenic zone at a deeper depth than 10 km (Protti et al., 2014).

The spatial variation of stress drops and interplate coupling at the plate boundary results from the heterogeneous distribution of frictional properties at the plate boundary in the Central American subduction zone. In addition, a low stress drop suggests a high pore pressure generated by the existence of fluids (Yao & Yang, 2020). Therefore, the frictional strength of the slow earthquake area at a depth range of 6–10 km can be quite weak owing to the rich fluid compared to that in the regions with regular and tsunami earthquakes.

In Costa Rica, repeating earthquakes occur around the large coseismic slip area of the 2012 M_W 7.6 earthquake on the Nicoya Peninsula (Chaves et al., 2020). In this study, VLFEs were mainly located near the trench axis, which is spatially separated from the locations of repeating earthquakes that occur near the Nicoya Peninsula. Such spatial separation of slow and repeating earthquakes on the plate boundary is also found in the Nankai (e.g., Takemura et al., 2020) and the Tohoku subduction zone (e.g., Nishikawa et al., 2019).

4.3. Comparison with other subduction zones

Our study revealed that shallow VLFEs and tremors occur near the trench axis off Costa Rica, in the updip of coseismic slip areas of thrust-type large earthquakes with an M_W of 7–8. In the updip area, SSEs also occurred in 2007–2012 (Dixon et al., 2017; Jiang et al., 2012). The depth range and the separate distribution between shallow slow earthquakes and large earthquakes off Costa Rica are similar to shallow slow earthquakes in the Nankai subduction zone, where slow earthquakes are spatially separated from high slip-deficit zones (e.g., Takemura et al., 2020). On the other hand, before the 2011 Tohoku earthquake, shallow slow slip events propagated to the initial rupture point of the great earthquake (Kato et al., 2012). Therefore, the characteristics of distribution of slow and large earthquakes differ between Tohoku and Costa Rica.

There are other common features in shallow slow earthquakes between Costa Rica and Nankai. Although the lower limit of M_W is large (~3.4) due to a strict threshold, the ranges of

405 magnitudes and source durations of shallow VLFEs off Costa Rica are similar to those of shallow
406 VLFEs in the Nankai subduction zones (e.g., Takemura et al., 2019). The recurrence intervals of
407 activation of slow earthquakes are one to several years in Costa Rica (Jiang et al., 2012), which is
408 similar to shallow slow earthquakes in the Nankai subduction zone, but different from the shorter
409 intervals of deep slow earthquakes in Nankai (e.g., Baba et al., 2020b). Although the tremor
410 analysis is limited due to the missing of small events by the strict threshold of VLFEs, the range
411 of energy rates of tremors was 10^3–$10^{5.5}$ J/s. The upper limit of the energy rate range of tremors is
412 similar to that observed for shallow tremors in Nankai (Yabe et al., 2019). The estimated scaled
413 energy of slow earthquakes off Costa Rica is also similar to that of shallow slow earthquakes in
414 the Nankai subduction zone (Yabe et al., 2019). The scaled energy is related to the rupture process
415 of seismic phenomena (Kanamori & Rivera, 2006); therefore, these results suggest that the
416 frictional properties within the shallow slow earthquake areas are similar in both Costa Rica and
417 Nankai. On the other hand, the scaled energy range in both regions is 0.5–1 orders of magnitude
418 larger than that of shallow slow earthquakes in the Tohoku subduction zone (Yabe et al., 2021),
419 and approximately 1 order of magnitude larger than that of deep slow earthquakes in Nankai (Ide
420 et al., 2008; Ide &Yabe, 2014; Ide, 2016; Ide & Maury, 2018; Maeda & Obara, 2009) (Figure 9).
421 We note that scaled energies of shallow slow earthquakes were estimated for individual events,
422 whereas those of deep slow earthquakes estimated by Ide &Yabe (2014), Ide (2016), and Ide &
423 Maury (2018) were estimated for stacked events.

424 The range of scaled energy and distribution of shallow slow earthquakes off Costa Rica are
425 more similar to those in shallow Nankai than shallow Tohoku. According to Syracuse et al. (2010),
426 the age and thermal parameters of Costa Rica are 15.8 Ma and 1,010 km, respectively, which are
427 closer to those of Nankai (20.0 Ma and 450 km, respectively) than Tohoku (115.2–130.5 Ma and
428 5,720–6,040 km, respectively). The thermal parameter, which is product of the incoming plate age,
429 the convergence rate, and the sine of the slab dip angle, is used to predict the slab surface
430 temperature at a given depth (e.g., Kirby et al., 1991; Syracuse et al., 2010). In addition, the
431 temperatures of shallower parts of plate interfaces of these subduction zones where shallow slow
432 earthquakes are not so different (Nankai: ~100 ºC in the depth range of 0–5 km from the seafloor;
433 Tohoku: 65–110 ºC in the depth range of 6–12 km; and Costa Rica: 12–60ºC in the depth range of
434 0–10 km; modeled temperature in Saffer & Wallace, 2015). On the other hand, the Central
435 American subduction zone is subduction of fast convergence rate (~8 cm/year; DeMets et al.,
436 1994), high dip angle, and erosional type (e.g., Bangs et al., 2016), which are more similar to
437 Tohoku than Nankai. Although the characteristics of slow earthquake activity can be related to
438 various factors, the thermal parameter and incoming plate age of Costa Rica is more similar to
439 Nankai than Tohoku. The temperature structure of the shallow plate interface is probably most
440 sensitive to incoming plate age (Maunder et al., 2019) and secondarily to thermal parameter
441 (Syracuse et al., 2010). Hence, similar temperature conditions on the interface may explain the
442 common features of shallow slow earthquakes off Costa Rica and in Nankai.

443 In previous studies, the large slip area of the SSE in 2007 was separated into deeper and
444 shallower parts (Jiang et al., 2017), and deep LFEs and tremors were detected downdip of the
445 seismogenic zone (Brown et al., 2009; Outerbridge et al., 2010). And, several VLFEs were located
446 in the downdip area, in the similar area reported in previous studies of tremors and LFEs. If these
447 deep VLFEs, LFEs and tremors occur in the downdip area, slow earthquakes might occur at
448 separate depths along both shallower and deeper extensions of rupture zones of large earthquakes
449 (Figure 10). This characteristic might also be the same as that of the Nankai subduction zone
450 (Obara & Kato, 2016). This suggests that the tectonic property may be similar in the wide depth

range in Costa Rica and Nankai. On the other hand, slow earthquakes are distributed only in the deeper part in the Cascadia subduction zone and only in the shallower part in the Tohoku subduction zone. The variation of the distribution of slow earthquakes may be attributed to the difference in tectonics or detection capability. The elucidation of the reason for the difference of the distribution in slow earthquake is future works.

5. Conclusions

Based on the grid-search matched-filter technique using synthetic templates in the regional 3D model, we detected and located VLFEs around the Nicoya Peninsula. Many VLFEs occurred in September 2004 and August 2005, and more than 90% of the VLFEs were located near the trench axis, where the plate boundary is at a depth range of 6–10 km, updip of the seismogenic zone, whereas several VLFEs were located in the downdip area at a depth of ~40 km. In this area, the occurrence of shallow SSEs is suggested by VLFE episodes. The region with VLFE activity overlaps with the shallower part of the large slip area of the 2007 SSE; therefore, the occurrences of shallow SSEs are suggested in September 2004 and August 2005 to occur in the same area as the shallower part of the 2007 SSE. The distribution of VLFEs lies in the gap surrounding coseismic slip areas of tsunami and large regular earthquakes. This separation reflects the spatial distribution of the frictional strength of the plate boundary in the Central American subduction zone. By using high-frequency seismogram envelopes, we also estimated the energy rates of tremors accompanying VLFEs. The ranges of magnitude and source duration of VLFEs, energy rate of tremors, and scaled energy off Costa Rica are similar to those in shallow slow earthquakes in the Nankai subduction zone.

Data Availability

We used seismograms of the TUCAN network (Abers & Fischer, 2003; https://doi.org/10.7914/SN/YO_2003) and Global Seismograph Network (Scripps Institution of Oceanography, 1986; https://doi.org/10.7914/SN/II). We used the earthquake catalog of the U.S. Geological Survey (https://earthquake.usgs.gov/earthquakes/search/). We used OpenSWPC code Version 5.0.2 (Maeda et al., 2017; https://doi.org/10.5281/zenodo.3712650) for the numerical simulations. Numerical simulations were conducted using the Fujitsu PRIMERGY CX600M1/CX1640M1 (Oakforest-PACS) at the Information Technology Center, the University of Tokyo. We used generic mapping tools (Wessel et al., 2013) and Seismic Analysis Code (Helfrich et al., 2013) to prepare the figures and process seismograms, respectively. The VLFE and tremor catalog constructed by this study is provided in an open access repository, zenodo (doi: 10.5281/zenodo.4435232).

Acknowledgements

We would like to thank the Editor Rachel Abercrombie, the Associate Editor Elisa Tinti, Alexandra A. Hutchison and two anonymous reviewers for their valuable comments and suggestions. We would like to thank Suguru Yabe for valuable discussions. We would also like to thank Marino Protti for providing the earthquake catalog in Costa Rica and for discussions. We thank Editage (www.editage.com) for English proofreading. This research was supported by JSPS KAKENHI Grant in Science Research on Innovative Areas “Science of Slow Earthquakes” (JP16H06473) and JSPS Research Fellowship DC1 (JP19J20760). This study was also supported by the ERI-JURP 2020-S-04.

References

Abers, G. A., & Fischer, K. M. (2003). Tomography Under Costa Rica and Nicaragua. International Federation of Digital Seismograph Networks. https://doi.org/10.7914/SN/YO_2003

Aki, K. (1980). Attenuation of shear-waves in the lithosphere for frequencies from 0.05 to 25 Hz. *Physics of the Earth and Planetary Interiors*, *21*(1), 50–60. https://doi.org/10.1016/0031-9201(80)90019-9

Amante, C., & Eakins, B.W. (2009). ETOPO1 1 Arc-Minute Global Relief Model: Procedures, Data Sources and Analysis. NOAA Technical Memorandum NESDIS NGDC-24. https://doi.org/10.7289/V5C8276M

Araki, E., Saffer, D. M., Kopf, A. J., Wallace, L. M., Kimura, T., Machida, Y., Ide, S., Davis, E., & IODP Expedition 365 shipboard scientists (2017). Recurring and triggered slow-slip events near the trench at the Nankai Trough subduction megathrust. *Science*, *356*(6343), 1157–1160. https://doi.org/10.1126/science.aan3120

Baba, S., Takeo, A., Obara, K., Kato, A., Maeda, T., & Matsuzawa, T. (2018). Temporal Activity Modulation of Deep Very Low Frequency Earthquakes in Shikoku, Southwest Japan. *Geophysical Research Letters*, *45*(2), 733–738. https://doi.org/10.1002/2017GL076122

Baba, S., Takeo, A., Obara, K., Matsuzawa, T., & Maeda, T. (2020a). Comprehensive Detection of Very Low Frequency Earthquakes Off the Hokkaido and Tohoku Pacific Coasts, Northeastern Japan. *Journal of Geophysical Research: Solid Earth*, *125*(1), 1–13. https://doi.org/10.1029/2019JB017988

Baba, S., Takemura, S., Obara, K., & Noda, A. (2020b). Slow Earthquakes Illuminating Interplate Coupling Heterogeneities in Subduction Zones. *Geophysical Research Letters*, *47*(14), 4–5. https://doi.org/10.1029/2020GL088089

Bangs, N. L., McIntosh, K. D., Silver, E. A., Kluesner, J. W., & Ranero, C. R. (2016). A recent phase of accretion along the southern Costa Rican subduction zone. *Earth and Planetary Science Letters*, *443*, 204–215. https://doi.org/10.1016/j.epsl.2016.03.008

Bilek, S. L., Rotman, H. M. M., & Phillips, W. S. (2016). Low stress drop earthquakes in the rupture zone of the 1992 Nicaragua tsunami earthquake. *Geophysical Research Letters*, *43*(19), 10,180-10,188. https://doi.org/10.1002/2016GL070409

Brown, J. R., Beroza, G. C., Ide, S., Ohta, K., Shelly, D. R., Schwartz, S. Y., et al. (2009). Deep low-frequency earthquakes in tremor localize to the plate interface in multiple subduction zones. *Geophysical Research Letters*, *36*(19), 1–5. https://doi.org/10.1029/2009GL040027

Brown, K. M., Tryon, M. D., DeShon, H. R., Dorman, L. R. M., & Schwartz, S. Y. (2005). Correlated transient fluid pulsing and seismic tremor in the Costa Rica subduction zone. *Earth and Planetary Science Letters*, *238*(1–2), 189–203. https://doi.org/10.1016/j.epsl.2005.06.055

Chaves, E. J., Schwartz, S. Y., & Abercrombie, R. E. (2020). Repeating earthquakes record fault weakening and healing in areas of megathrust postseismic slip. *Science Advances,* 6(32), eaaz9317. https://doi.org/10.1126/sciadv.aaz9317

Christensen, N. I., & Salisbury, M. H. (1975). Structure and constitution of the lower oceanic crust. *Reviews of Geophysics*, *13*(1), 57–86. https://doi.org/10.1029/RG013i001p00057

Davis, E., Heesemann, M., & Wang, K. (2011). Evidence for episodic aseismic slip across the subduction seismogenic zone off Costa Rica: CORK borehole pressure observations at the

subduction prism toe. *Earth and Planetary Science Letters*, *306*(3–4), 299–305. https://doi.org/10.1016/j.epsl.2011.04.017

Davis, E. E., Villinger, H., & Sun, T. (2015). Slow and delayed deformation and uplift of the outermost subduction prism following ETS and seismogenic slip events beneath Nicoya Peninsula, Costa Rica. *Earth and Planetary Science Letters*, *410*, 117–127. https://doi.org/10.1016/j.epsl.2014.11.015

DeMets, C., Gordon, R. G., Argus, D. F., & Stein, S. (1994). Effect of recent revisions to the geomagnetic reversal time scale on estimates of current plate motions. *Geophysical Research Letters*, *21*(20), 2191–2194. https://doi.org/10.1029/94GL02118

Dixon, T. H., Jiang, Y., Malservisi, R., McCaffrey, R., Voss, N., Protti, M., & Gonzalez, V. (2014). Earthquake and tsunami forecasts: Relation of slow slip events to subsequent earthquake rupture. *Proceedings of the National Academy of Sciences of the United States of America*, *111*(48), 17039–17044. https://doi.org/10.1073/pnas.1412299111

Dragert, H., Wang, K., James, T. S. (2001). A Silent Slip Event on the Deeper Cascadia Subduction Interface. *Science*, *292*(5521), 1525–1528. https://doi.org/10.1126/science.1060152

Feng, L., Newman, A. V., Protti, M., Gonzlez, V., Jiang, Y., & Dixon, T. H. (2012). Active deformation near the Nicoya Peninsula, northwestern Costa Rica, between 1996 and 2010: Interseismic megathrust coupling. *Journal of Geophysical Research: Solid Earth*, *117*(6), 1–23. https://doi.org/10.1029/2012JB009230

Ghosh, A., Huesca-Pérez, E., Brodsky, E., & Ito, Y. (2015). Very low frequency earthquakes in Cascadia migrate with tremor. *Geophysical Research Letters*, *42*(9), 3228–3232. https://doi.org/10.1002/2015GL063286

Gomberg, J., Wech, A., Creager, K., Obara, K., & Agnew, D. (2016). Reconsidering earthquake scaling. *Geophysical Research Letters*, *43*(12), 6243–6251. https://doi.org/10.1002/2016GL069967

Hawthorne, J. C., & Bartlow, N. M. (2018). Observing and Modeling the Spectrum of a Slow Slip Event. *Journal of Geophysical Research: Solid Earth*, *123*(5), 4243–4265. https://doi.org/10.1029/2017JB015124

Hasselmann, K. (1963). A statistical analysis of the generation of microseisms. *Reviews of Geophysics*, 1, 177–209. https://doi.org/10.1029/RG001i002p00177

Hayes, G. P., Moore, G. L., Portner, D. E., Hearne, M., Flamme, H., Furtney, M., & Smoczyk, G. M. (2018). Slab2, a Comprehensive Subduction Zone Geometry Model, *Science*, 61(October), 58–61. https://doi.org/10.1126/science.aat4723

Helffrich, G., Wookey, J., & Bastow, I. (2013). The Seismic Analysis Code. Cambridge: Cambridge University Press. https://doi.org/10.1017/CBO9781139547260

Hutchison, A. A. (2020). Interepisodic Tremor and Slip Event Episodes of Quasi-spatiotemporally Discrete Tremor and Very Low Frequency Earthquakes in Cascadia Suggestive of a Connective Underlying, Heterogeneous Process. *Geophysical Research Letters*, *47*(3), 1–7. https://doi.org/10.1029/2019GL086798

Hutchison, A. A., & Ghosh, A. (2016). Very low frequency earthquakes spatiotemporally asynchronous with strong tremor during the 2014 episodic tremor and slip event in Cascadia. *Geophysical Research Letters*, *43*(13), 6876–6882. https://doi.org/10.1002/2016GL069750

582 Hutchison, A. A., & Ghosh, A. (2019). Repeating VLFEs During ETS Events in Cascadia Track
583 Slow Slip and Continue Throughout Inter-ETS Period. *Journal of Geophysical Research:*
584 *Solid Earth*, *124*(1), 554–565. https://doi.org/10.1029/2018JB016138
585 Ide, S. (2016). Characteristics of slow earthquakes in the very low frequency band: Application
586 to the Cascadia subduction zone. *Journal of Geophysical Research: Solid Earth*, *121*(8),
587 5942–5952. https://doi.org/10.1002/2016JB013085
588 Ide, S., & Maury, J. (2018). Seismic Moment, Seismic Energy, and Source Duration of Slow
589 Earthquakes: Application of Brownian slow earthquake model to three major subduction
590 zones. *Geophysical Research Letters*, *45*(7), 3059–3067.
591 https://doi.org/10.1002/2018GL077461
592 Ide, S., & Yabe, S. (2014). Universality of slow earthquakes in the very low frequency band.
593 *Geophysical Research Letters*, *41*(8), 2786–2793. https://doi.org/10.1002/2014GL059712
594 Ide, S., Beroza, G. C., Shelly, D. R., & Uchide, T. (2007). A scaling law for slow earthquakes.
595 *Nature*, *447*(7140), 76–79. https://doi.org/10.1038/nature05780
596 Ide, S., Imanishi, K., Yoshida, Y., Beroza, G. C., & Shelly, D. R. (2008). Bridging the gap
597 between seismically and geodetically detected slow earthquakes. *Geophysical Research*
598 *Letters*, *35*(10), 2–7. https://doi.org/10.1029/2008GL034014
599 Ito, Y., Obara, K., Shiomi, K., Sekine, S., & Hirose, H. (2007). Slow Earthquakes Coincident
600 with Episodic Tremors and Slow Slip Events. *Science*, *315*(5811), 503–506.
601 https://doi.org/10.1126/science.1134454
602 Ito, Y., & Obara, K. (2006). Very low frequency earthquakes within accretionary prisms are very
603 low stress-drop earthquakes. *Geophysical Research Letters*, *33*(9), 1–4.
604 https://doi.org/10.1029/2006GL025883
605 Ito, Y., Obara, K., Matsuzawa, T., & Maeda, T. (2009). Very low frequency earthquakes related
606 to small asperities on the plate boundary interface at the locked to aseismic transition.
607 *Journal of Geophysical Research: Solid Earth*, *114*(11), 1–16.
608 https://doi.org/10.1029/2008JB006036
609 Ito, Y., Hino, R., Kido, M., Fujimoto, H., Osada, Y., Inazu, D., et al. (2013). Episodic slow slip
610 events in the Japan subduction zone before the 2011 Tohoku-Oki earthquake.
611 *Tectonophysics*, *600*, 14–26. https://doi.org/10.1016/j.tecto.2012.08.022
612 Jiang, Y., Wdowinski, S., Dixon, T. H., Hackl, M., Protti, M., & Gonzalez, V. (2012). Slow slip
613 events in Costa Rica detected by continuous GPS observations, 2002-2011. *Geochemistry,*
614 *Geophysics, Geosystems*, *13*(1), 1–18. https://doi.org/10.1029/2012GC004058
615 Jiang, Y., Liu, Z., Davis, E. E., Schwartz, S. Y., Dixon, T. H., Voss, N., et al. (2017). Strain
616 release at the trench during shallow slow slip: The example of Nicoya Peninsula, Costa
617 Rica. *Geophysical Research Letters*, *44*(10), 4846–4854.
618 https://doi.org/10.1002/2017GL072803
619 Kanamori, H., & Rivera, L. (2006). Energy partitioning during an earthquake. *Geophysical*
620 *Monograph Series*, *170*, 3–13. https://doi.org/10.1029/170GM03
621 Kaneko, L., Ide, S., & Nakano, M. (2018). Slow Earthquakes in the Microseism Frequency Band
622 (0.1–1.0 Hz) off Kii Peninsula, Japan. *Geophysical Research Letters*, *45*(6), 2618–2624.
623 https://doi.org/10.1002/2017GL076773
624 Kato, A., & Nakagawa, S. (2014). Geophysical Research Letters. *Geophysical Research Letters*,
625 (April), 6413–6419. https://doi.org/10.1002/2014GL061184.Received

Kato, A., Obara, K., Igarashi, T., Tsuruoka, H., Nakagawa, S., & Hirata, N. (2012). Propagation of Slow Slip Leading Up to the 2011 Mw 9.0 Tohoku-Oki Earthquake. *Science*, *335*(6069), 705–708. https://doi.org/10.1126/science.1215141

Kirby, S. T., Durham, W. B., & Stern, L. A. (1991). Mantle Phase Changes and Deep-Earthquake Faulting in Subducting Lithosphere. *Science*, 252(5003), 216-225. https://doi.org/10.1126/science.252.5003.216

Laske, G., Masters., G., Ma, Z., & Pasyanos, M. (2013). Update on CRUST1.0 - A 1-degree Global Model of Earth's Crust, Paper presented at EGU General Assembly, European Geoscience Union, Vienna

Maeda, T., & Obara, K. (2009). Spatiotemporal distribution of seismic energy radiation from low-frequency tremor in western Shikoku, Japan. *Journal of Geophysical Research: Solid Earth*, *114*(10). https://doi.org/10.1029/2008JB006043

Maeda, T., Takemura, S., & Furumura, T. (2017). OpenSWPC: An open-source integrated parallel simulation code for modeling seismic wave propagation in 3D heterogeneous viscoelastic media 4. Seismology. *Earth, Planets and Space*, *69*(1). https://doi.org/10.1186/s40623-017-0687-2

Malservisi, R., Schwartz, S.Y., Voss, N., Protti, M., Gonzalez, V., Dixon, T.H., Jian, Y., Newman, A.V., Walter, J.I., & Voyenko, D. (2015). Multiscale postseismic behavior on a megathrust: The 2012 Nicoya earthquake, Costa Rica. *Geochemistry, Geophysics, Geosystems*, 16, 1848–1864. https://doi.org/10.1002/2015GC005794.

Maunder, B., van Hunen, J., Bouilhol, P., & Magni, V. (2019). Modeling Slab Temperature: A Reevaluation of the Thermal Parameter. *Geochemistry, Geophysics, Geosystems*, *20*(2), 673–687. https://doi.org/10.1029/2018GC007641

Nadeau, R. M., & Dolenc, D. (2005). Nonvolcanic tremors deep beneath the San Andreas Fault. *Science*, *307*(5708), 389. https://doi.org/10.1126/science.1107142

Nakano, M., Hori, T., Araki, E., Kodaira, S., & Ide, S. (2018). Shallow very-low-frequency earthquakes accompany slow slip events in the Nankai subduction zone /704/2151/210 /704/2151/508 article. *Nature Communications*, *9*(1). https://doi.org/10.1038/s41467-018-03431-5

Nishikawa, T., Matsuzawa, T., Ohta, K., Uchida, N., Nishimura, T., & Ide, S. (2019). The slow earthquake spectrum in the Japan Trench illuminated by the S-net seafloor observatories. *Science (New York, N.Y.)*, *365*(6455), 808–813. https://doi.org/10.1126/science.aax5618

Obara, K. (2002). Nonvolcanic Deep Tremor Associated with Subduction in Southwest Japan. *Science*, *296*(5573), 1679–1681. https://doi.org/10.1126/science.1070378

Obara, K. (2011). Characteristics and interactions between non-volcanic tremor and related slow earthquakes in the Nankai subduction zone, southwest Japan. *Journal of Geodynamics*, *52*(3–4), 229–248. https://doi.org/10.1016/j.jog.2011.04.002

Obara, K., & Ito, Y. (2005). Very low frequency earthquakes excited by the 2004 off Kii peninsula earthquakes: A dynamic deformation process in the large accretionary prism. *Earth, Planets and Space*, *57*(4), 321–326. https://doi.org/10.1186/BF03352570

Obara, K., & Kato, A. (2016). Connecting slow earthquakes to huge earthquakes. *Science (New York, N.Y.)*, *353*(6296), 253–257. https://doi.org/10.1126/science.aaf1512

Outerbridge, K. C., Dixon, T. H., Schwartz, S. Y., Walter, J. I., Protti, M., Gonzalez, V., et al. (2010). A tremor and slip event on the Cocos-Caribbean subduction zone as measured by a global positioning system (GPS) and seismic network on the Nicoya Peninsula, Costa Rica.

Journal of Geophysical Research: Solid Earth, *115*(10), 1–17. https://doi.org/10.1029/2009JB006845

Protti, M. (1995). The March 25, 1990 (Mw=7.0, ML=6.8), earthquake at the entrance of the Nicoya Gulf, Costa Rica: its prior activity, foreshocks, aftershocks, and triggered seismicity. *Journal of Geophysical Research*, *100*(B10), 345–358. https://doi.org/10.1029/94jb03099

Protti, M., González, V., Newman, A. V., Dixon, T. H., Schwartz, S. Y., Marshall, J. S., et al. (2014). Nicoya earthquake rupture anticipated by geodetic measurement of the locked plate interface. *Nature Geoscience*, *7*(2), 117–121. https://doi.org/10.1038/ngeo2038

Rogers, G., & Dragert, H. (2003). Episodic Tremor and Slip on the Cascadia Subduction Zone: The Chatter of Silent Slip. *Science*, *300*(5627), 1942–1943. https://doi.org/10.1126/science.1084783

Rost, S., & Thomas, C. (2002). Array seismology: Methods and applications. *Reviews of Geophysics*, *40*(3), 2-1-2–27. https://doi.org/10.1029/2000RG000100

Ruiz, S., Aden-Antoniow, F., Baez, J. C., Otarola, C., Potin, B., del Campo, F., et al. (2017). Nucleation Phase and Dynamic Inversion of the M w 6.9 Valparaíso 2017 Earthquake in Central Chile. *Geophysical Research Letters*, *44*(20), 10,290-10,297. https://doi.org/10.1002/2017GL075675

Saffer, D. M., & Wallace, L. M. (2015). The frictional, hydrologic, metamorphic and thermal habitat of shallow slow earthquakes. *Nature Geoscience*, *8*(8), 594–600. https://doi.org/10.1038/ngeo2490

Satake, K. (1994). Mechanism of the 1992 Nicaragua Tsunami Earthquake. *Geophysical Research Letters*, *21*(23), 2519–2522. https://doi.org/10.1029/94GL02338

Sato, H., Fehler, M., & Maeda, T. (2012). Seismic Wave Propagation and Scattering in the Heterogeneous Earth Structure, 2nd ed., New York, Springer-Verlag.

Scripps Institution of Oceanography. (1986). IRIS/IDA Seismic Network. International Federation of Digital Seismograph Networks. https://doi.org/10.7914/SN/II

Shelly, D. R., Beroza, G. C., Ide, S., & Nakamula, S. (2006). Low-frequency earthquakes in Shikoku, Japan, and their relationship to episodic tremor and slip. *Nature*, *442*(7099), 188–191. https://doi.org/10.1038/nature04931

Shelly, D. R., Beroza, G. C., & Ide, S. (2007). Non-volcanic tremor and low-frequency earthquake swarms. *Nature*, *446*(7133), 305–307. https://doi.org/10.1038/nature05666

Solomon, E. A., Kastner, M., Wheat, C. G., Jannasch, H., Robertson, G., Davis, E. E., & Morris, J. D. (2009). Long-term hydrogeochemical records in the oceanic basement and forearc prism at the Costa Rica subduction zone. *Earth and Planetary Science Letters*, *282*(1–4), 240–251. https://doi.org/10.1016/j.epsl.2009.03.022

Sugioka, H., Okamoto, T., Nakamura, T., Ishihara, Y., Ito, A., Obana, K., et al. (2012). Tsunamigenic potential of the shallow subduction plate boundary inferred from slow seismic slip. *Nature Geoscience*, *5*(6), 414–418. https://doi.org/10.1038/ngeo1466

Syracuse, E. M., van Keken, P. E., Abers, G. A., Suetsugu, D., Bina, C., Inoue, T., et al. (2010). The global range of subduction zone thermal models. *Physics of the Earth and Planetary Interiors*, *183*(1–2), 73–90. https://doi.org/10.1016/j.pepi.2010.02.004

Takemura, S., Kobayashi, M., & Yoshimoto, K. (2017). High-frequency seismic wave propagation within the heterogeneous crust: Effects of seismic scattering and intrinsic attenuation on ground motion modelling. *Geophysical Journal International*, *210*(3), 1806–1822. https://doi.org/10.1093/gji/ggx269

Takemura, S., Matsuzawa, T., Noda, A., Tonegawa, T., Asano, Y., Kimura, T., & Shiomi, K. (2019). Structural Characteristics of the Nankai Trough Shallow Plate Boundary Inferred From Shallow Very Low Frequency Earthquakes. *Geophysical Research Letters*, *46*(8), 4192–4201. https://doi.org/10.1029/2019GL082448

Takemura, S., Okuwaki, R., Kubota, T., Shiomi, K., Kimura, T., & Noda, A. (2020). Centroid moment tensor inversions of offshore earthquakes using a three-dimensional velocity structure model: slip distributions on the plate boundary along the Nankai Trough. *Geophysical Journal International*, *222*(2), 1109–1125. https://doi.org/10.1093/gji/ggaa238

Tamaribuchi, K., Kobayashi, A., Nishimiya, T., Hirose, F., & Annoura, S. (2019). Characteristics of Shallow Low-Frequency Earthquakes off the Kii Peninsula, Japan, in 2004 Revealed by Ocean Bottom Seismometers. *Geophysical Research Letters*, *46*(23), 13737–13745. https://doi.org/10.1029/2019GL085158

Voss, N., Dixon, T. H., Liu, Z., Malservisi, R., Protti, M., & Schwartz, S. (2018). Do slow slip events trigger large and great megathrust earthquakes? *Science Advances*, *4*(10), 1–6. https://doi.org/10.1126/sciadv.aat8472

Voss, N. K., Malservisi, R., Dixon, T. H., & Protti, M. (2017). Slow slip events in the early part of the earthquake cycle. *Journal of Geophysical Research: Solid Earth*, *122*(8), 6773–6786. https://doi.org/10.1002/2016JB013741

Walter, J. I., Schwartz, S. Y., Protti, J. M., & Gonzalez, V. (2011). Persistent tremor within the northern Costa Rica seismogenic zone. *Geophysical Research Letters*, *38*(1), 1–5. https://doi.org/10.1029/2010GL045586

Walter, J. I., Schwartz, S. Y., Protti, M., & Gonzalez, V. (2013). The synchronous occurrence of shallow tremor and very low frequency earthquakes offshore of the Nicoya Peninsula, Costa Rica. *Geophysical Research Letters*, *40*(8), 1517–1522. https://doi.org/10.1002/grl.50213

Wang, L., & Barbot, S. (2020). Excitation of San Andreas tremors by thermal instabilities below the seismogenic zone. *Science Advances*, *6*(36). https://doi.org/10.1126/sciadv.abb2057

Wessel, P., Smith, W. H. F., Scharroo, R., Luis, J., & Wobbe, F. (2013). Generic mapping tools: Improved version released. *Eos*, *94*(45), 409–410. https://doi.org/10.1002/2013EO450001

Xie, S., Dixon, T. H., Malservisi, R., Jiang, Y., Protti, M., & Muller, C. (2020). Slow Slip and Inter-transient Locking on the Nicoya Megathrust in the Late and Early Stages of an Earthquake Cycle. *Journal of Geophysical Research: Solid Earth*, *125*(11), 1–22. https://doi.org/10.1029/2020JB020503

Yabe, S., Tonegawa, T., & Nakano, M. (2019). Scaled Energy Estimation for Shallow Slow Earthquakes. *Journal of Geophysical Research: Solid Earth*, *124*(2), 1507–1519. https://doi.org/10.1029/2018JB016815

Yabe, S., Baba, S., Tonegawa, T., Nakano, M., & Takemura, S. (2021). Seismic energy radiation and along-strike heterogeneities of shallow tectonic tremors at the Nankai Trough and Japan Trench. *Tectonophysics*, 228714. https://doi.org/10.1016/j.tecto.2020.228714

Yao, S., & Yang, H. (2020). Rupture Dynamics of the 2012 Nicoya Mw 7.6 Earthquake: Evidence for Low Strength on the Megathrust. *Geophysical Research Letters*, *47*(13), 1–11. https://doi.org/10.1029/2020GL087508

Yokota, Y., & Ishikawa, T. (2020). Shallow slow slip events along the Nankai Trough detected by GNSS-A. *Science Advances*, *6*(3), 1–12. https://doi.org/10.1126/sciadv.aay5786

Yoshimoto, K., Sato, H., & Ohtake, M. (1993). Frequency-Dependent Attenuation of P and S Waves In the Kanto Area, Japan, Based On the Coda-Normalization Method. *Geophysical*

Journal International, *114*(1), 165–174. https://doi.org/10.1111/j.1365-246X.1993.tb01476.x

Yue, H., Lay, T., Schwartz, S. Y., Rivera, L., Protti, M., Dixon, T. H., et al. (2013). The 5 September 2012 Nicoya, Costa Rica Mw 7.6 earthquake rupture process from joint inversion of high-rate GPS, strong-motion, and teleseismic P wave data and its relationship to adjacent plate boundary interface properties. *Journal of Geophysical Research: Solid Earth*, *118*(10), 5453–5466. https://doi.org/10.1002/jgrb.50379

Figures

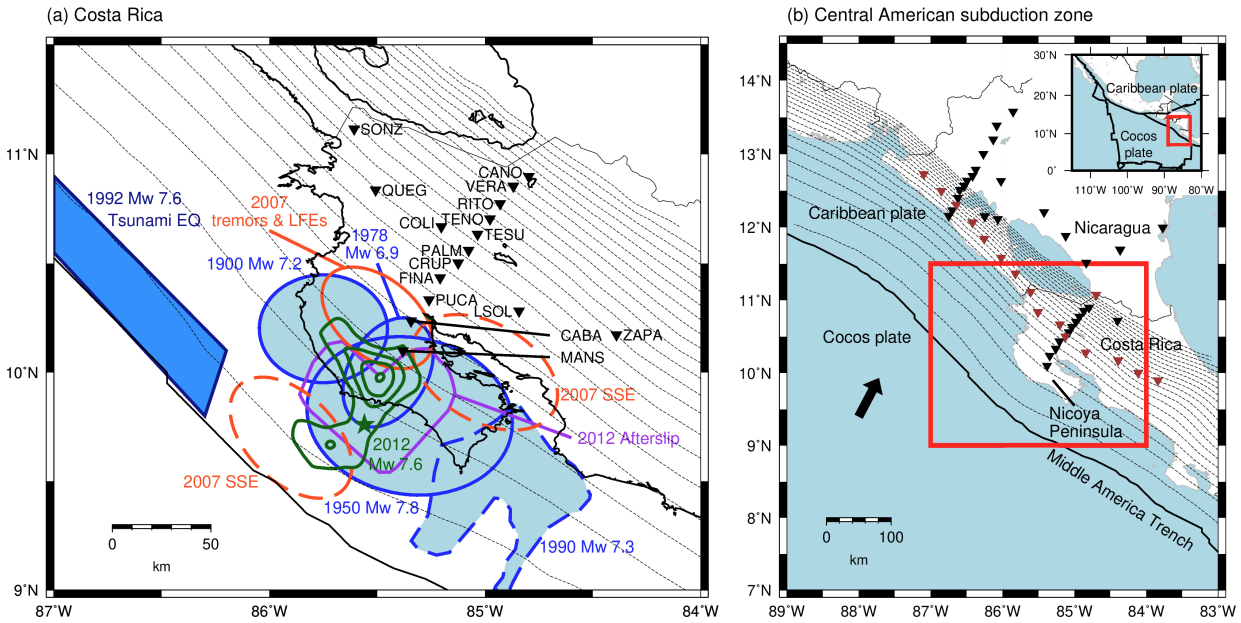

Figure 1. (a) Large regular and slow earthquake areas based on previous studies around the Nicoya Peninsula, in Costa Rica. Green contours show the coseismic slip distribution of the 2012 M_W 7.6 earthquake with a 1-m interval (Yue et al., 2013). Blue areas show the slip areas of large regular earthquakes (1990 M_W 7.3: Protti et al., 1995 (surrounded by dashed blue line); others: Yue et al., 2013 (surrounded by solid blue lines)). Dark blue area surrounded by solid dark blue line indicate the slip area of the 1992 tsunami earthquake (Satake, 1994). Orange ellipses with dashed lines show large slip areas of the 2007 SSE, which were separated in updip and downdip areas (Jiang et al., 2017). The orange ellipse with a solid line shows the distributions of LFEs (Brown et al., 2009) and tremors (Outerbridge et al., 2010). The purple polygon shows the area whose afterslip of the 2012 M_W 7.6 earthquake is more than 150 mm (Malvervisi et al., 2015). Black inverted triangles show the station locations of the TUCAN network used in VLFE detection (Section 2.2). Dashed contours indicate the isodepths of the top of the Cocos Plate with 10 km intervals (Slab2; Hayes et al., 2018). (b) Map of the Central American subduction zone. Solid line represents the Middle America Trench (Slab2; Hayes et al., 2018). Dashed contours are the same as (a). Black arrow indicates the convergence direction of the Cocos Plate, which subducts below the Caribbean plate from the Middle America Trench (NUVEL-1A; DeMets et al., 1994). Inverted triangles show the locations of stations of the TUCAN network. Brown triangles are stations which were used in beamforming (Section 2.3). The black lines in the inset show plate boundaries.

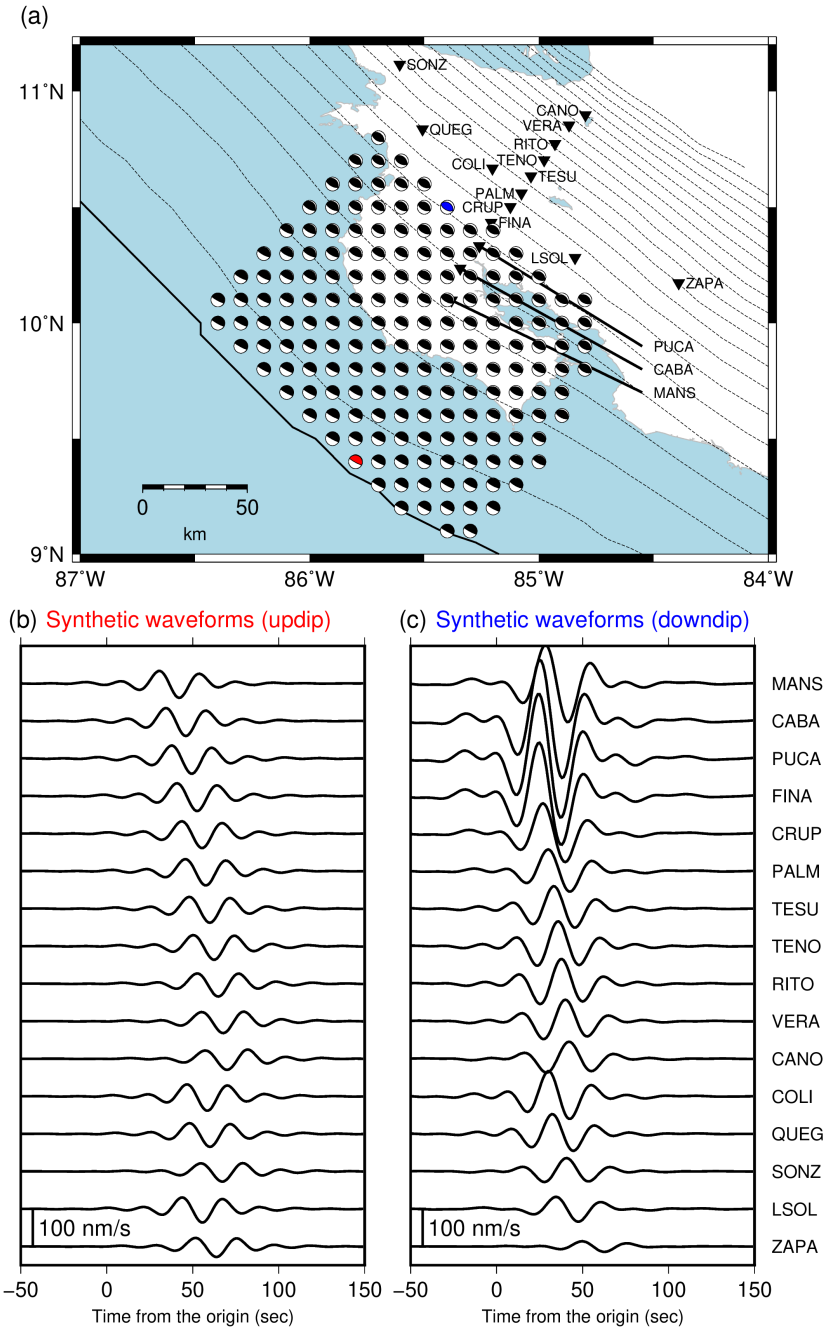

Figure 2. (a) Virtual source grids assumed in this study. Beach balls show the locations and focal mechanisms of the virtual sources. Inverted triangles and the black line are the same as in Figure 1. Dashed contours indicate the isodepths of the top of the Cocos Plate with 10 km intervals (Slab2; Hayes et al., 2018). Examples of waveforms of virtual sources with Mw 4 in the (b) updip and (c) downdip areas. Sources of Figures 1b and 1c are shown by the red and blue beachballs in Figure 2a, respectively. Amplitudes of the updip source are small due to the long distance between the source and stations, whereas amplitudes of the downdip source in the stations near the Nicoya Peninsula are large due to the short distance between the source and stations.

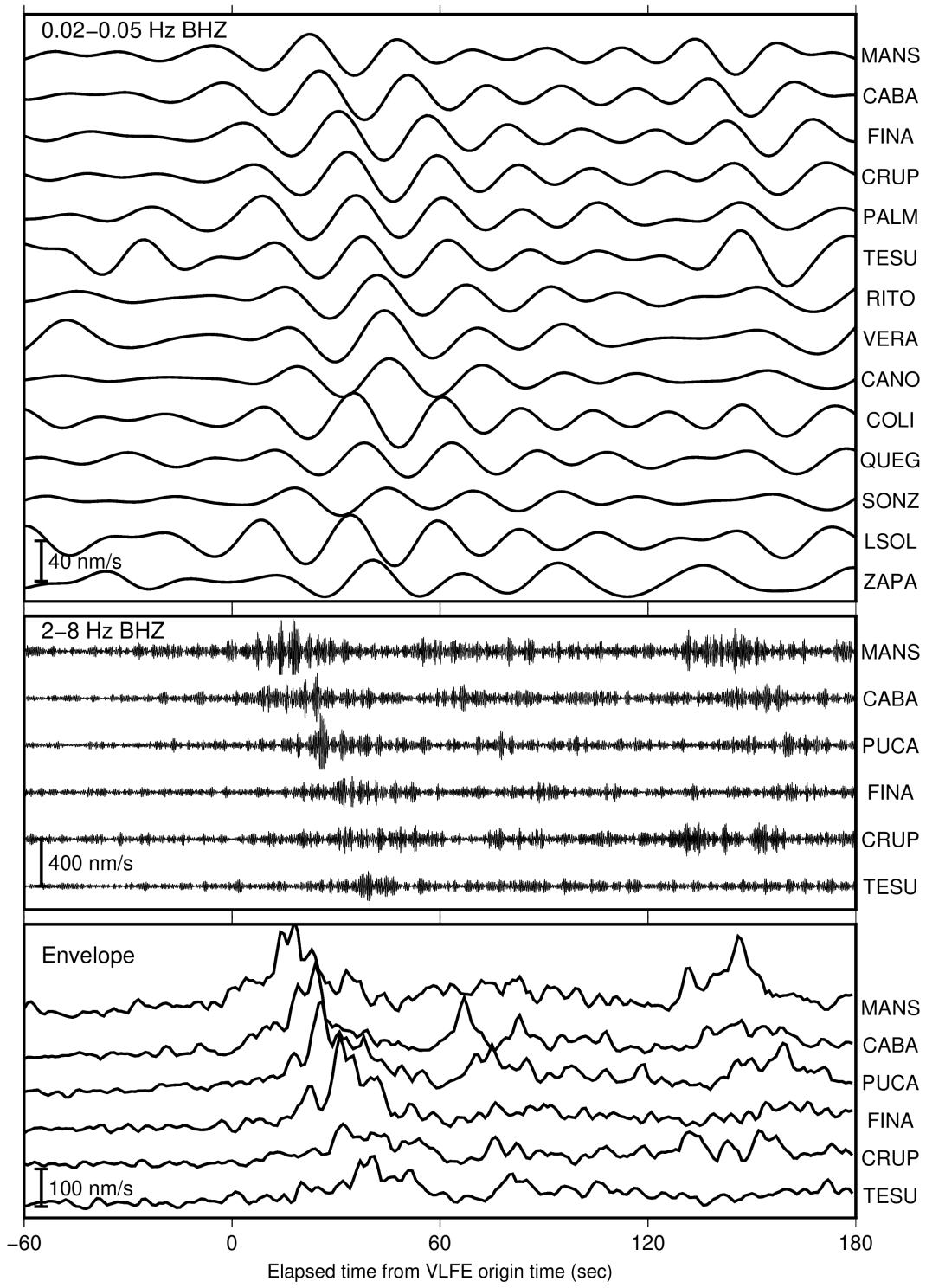

Figure 3. Example of waveforms of a VLFE and the corresponding tremor located at 85.8°W and 9.4°N (shown by a red beachball in Figure 2a) in the frequency range of 0.02–0.05 Hz and 2–8 Hz, and smoothed root-mean-square envelope in the frequency range of 2–8 Hz. Seismograms are shown from the origin time of the VLFE, 03:53:47 (UTC), August 10, 2005.

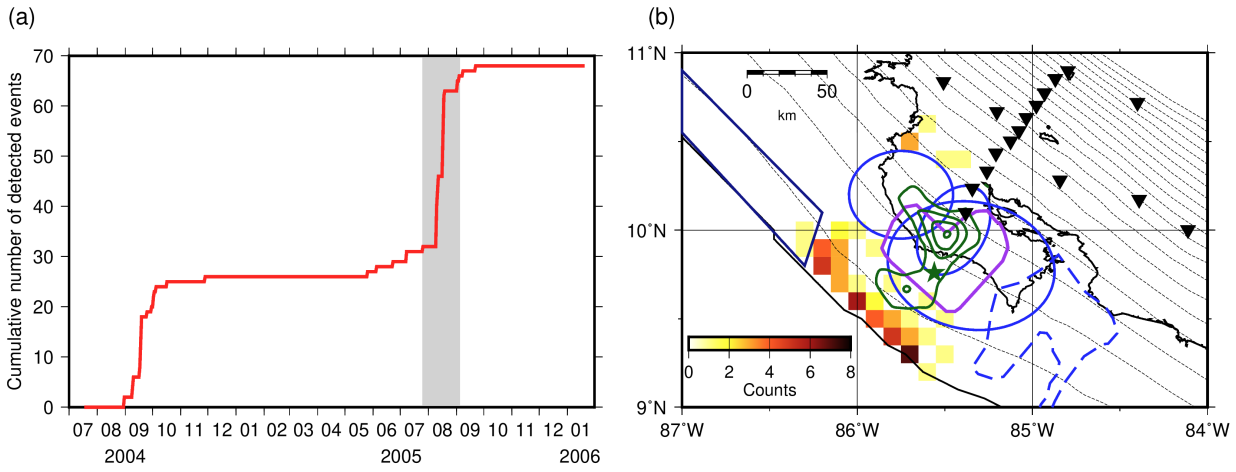

Figure 4. (a) Cumulative number of the VLFEs from July 2004 to January 2006. Gray shading shows the period of the 2005 SSE (Jiang et al., 2012). (b) Distribution of the number of detected events at each virtual source. Blue ellipses and polygons, dark blue quadrangle, inverted triangles, black line, the purple polygon, and dashed contours are the same as in Figure 1.

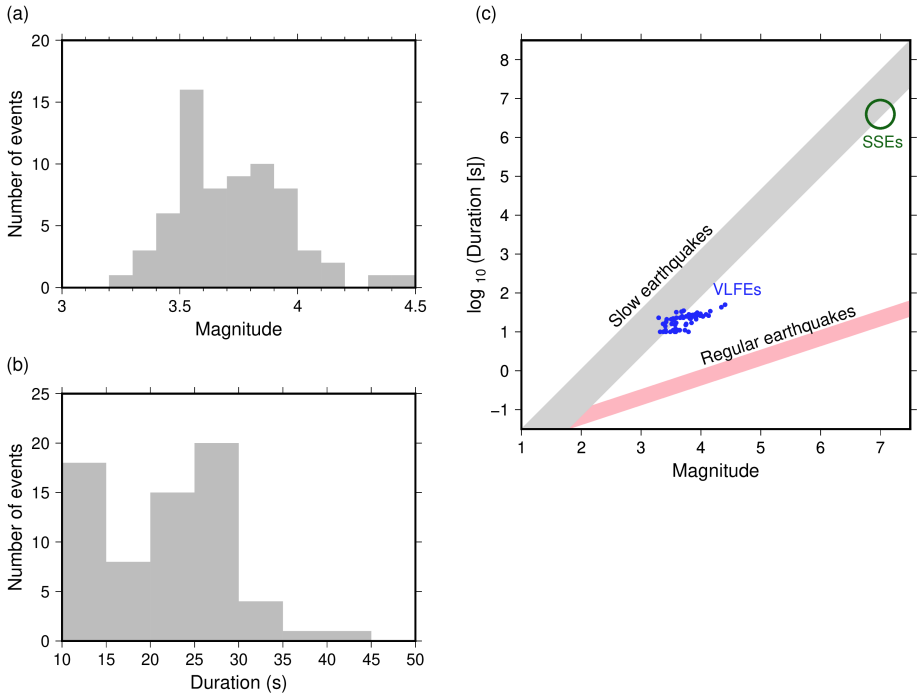

Figure 5. Distribution of (a) magnitudes and (b) source durations of VLFEs. (c) Relationship between durations and magnitudes of slow earthquakes. Gray and pink shadings show the ranges of the scaling law for slow and regular earthquakes by Ide et al. (2007). Blue dots indicate the relationship between source durations and magnitudes of VLFEs located in this study. Green circle represents the relationship between durations and magnitudes of SSEs in Costa Rica (Jiang et al., 2012; Voss et al., 2017).

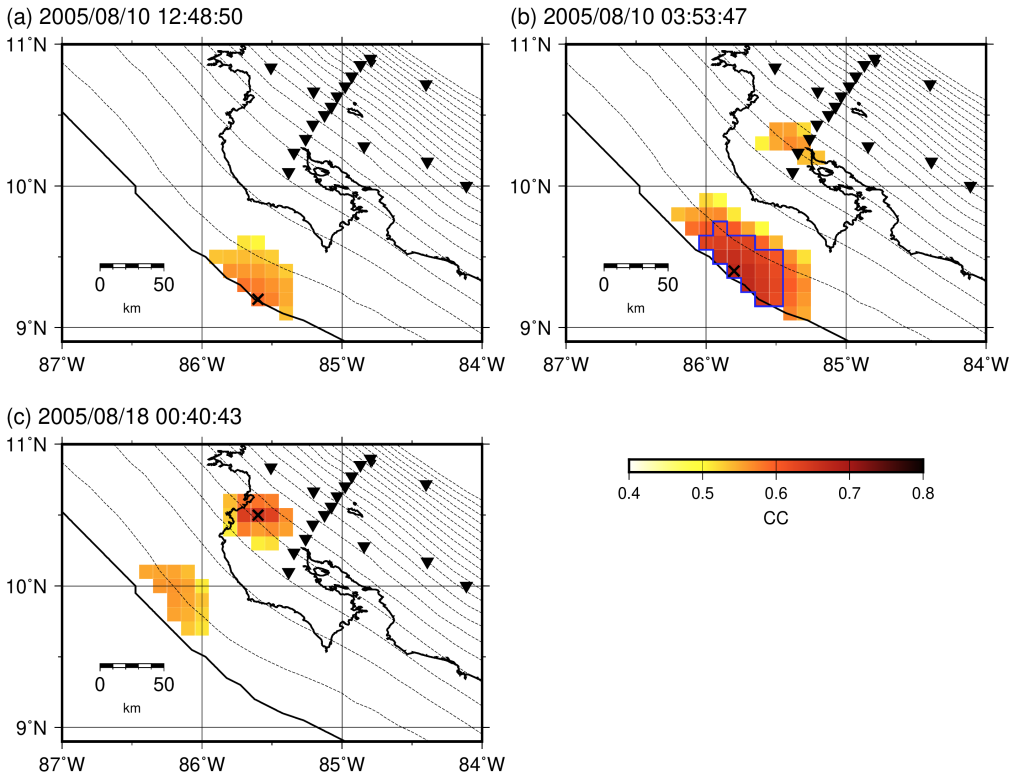

Figure 6. Examples of CC distributions of (a) an event which has large CCs only in updip grids, (b) an event which has large CCs both in updip and downdip grids but is located in an updip grid, and (c) an event which has large CCs both in updip and downdip grids but is located in a downdip grid. Cross mark in each map indicates the epicenter of the VLFE. Inverted triangles, black line, and dashed contours are the same as in Figure 1. The blue polygon in (b) indicates the grids whose CC are more than 0.9 times of the maximum CC.

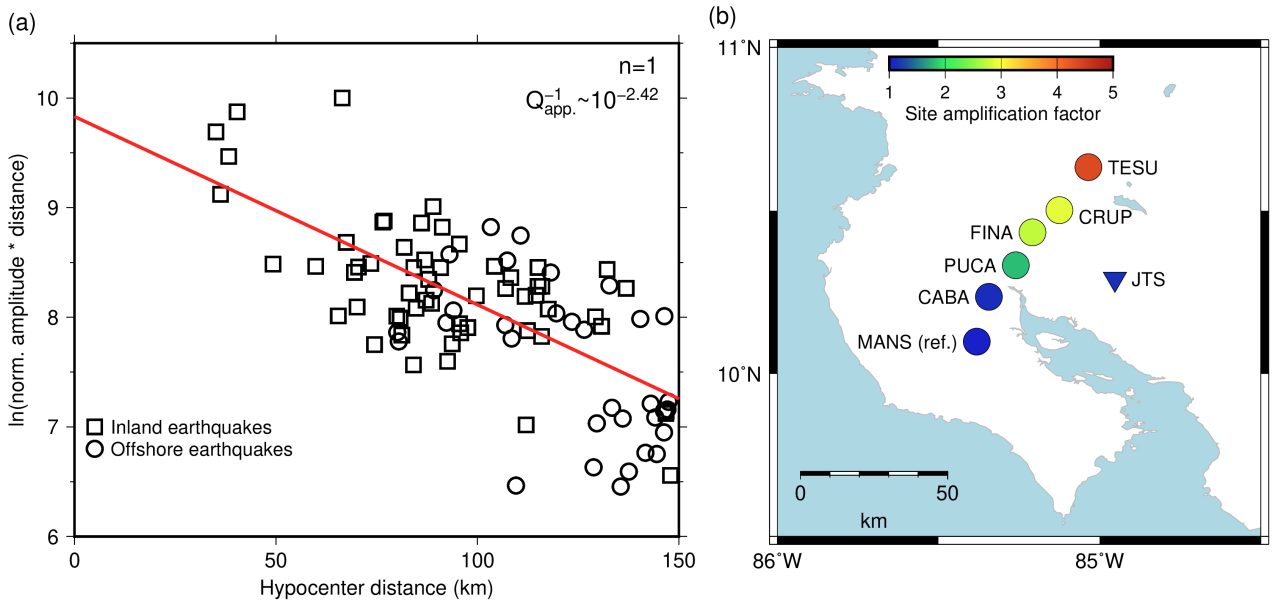

822

823 **Figure 7.** (a) Relationship between logarithm of coda-normalized maximum *S*-wave amplitudes
824 and hypocentral distances. To eliminate effects of geometrical spreading of *S*-wave, coda-
825 nomadized *S*-wave amplitudes were multiplied by their hypocentral distance. Red line shows the
826 regression line using Equation (2). (b) Site amplification factors relative to MANS based on
827 relative coda amplitude measurements.

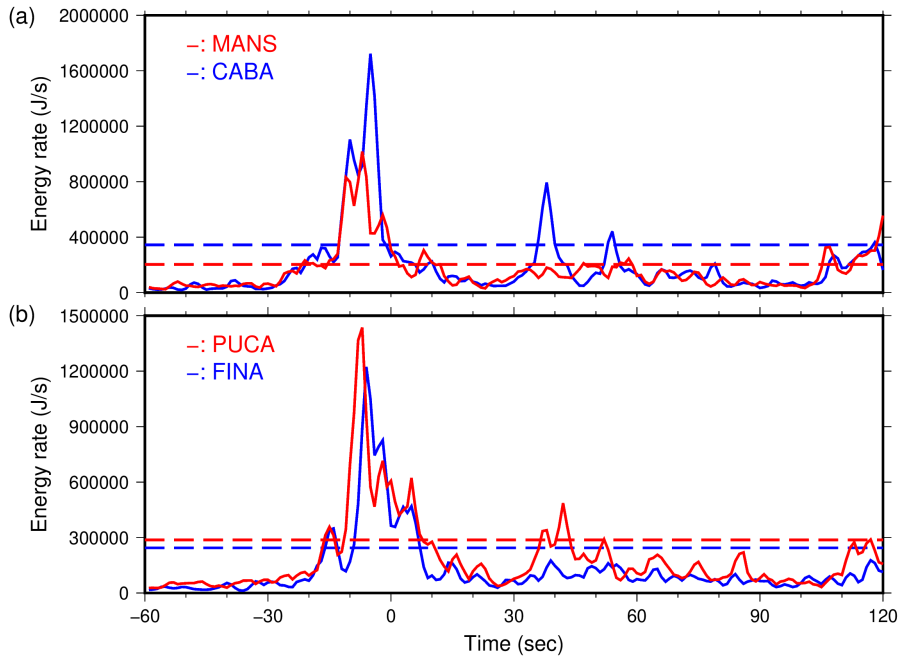

828

829 **Figure 8.** Temporal changes of energy rate functions of a tremor in (a) MANS and CABA and (b)
830 PUCA and FINA. The corresponding VLFE occurs on 03:53:47 (UTC), August 10, 2012. Dashed
831 lines indicate the threshold, which is set as 20% of the maximum value of the energy rate functions.

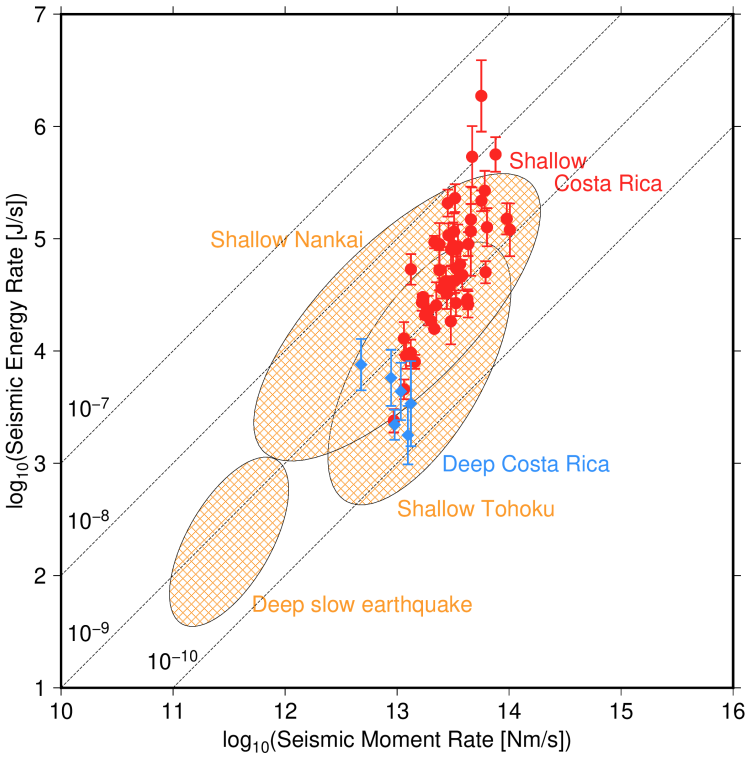

832

833 **Figure 9.** Relationship between seismic moment rates of VLFEs and seismic energy rates of
834 tremors estimated in this study. Red circles and blue diamonds show the events of updip and
835 downdip regions, respectively. Dashed lines show scaled energies of 10^{-7}, 10^{-8}, 10^{-9}, and 10^{-10}.
836 Orange shadings show the relationships between seismic moment rates of VLFEs and seismic
837 moment rates of tremors of shallow slow earthquakes in the Nankai (Yabe et al., 2019) and Tohoku
838 subduction zones (Yabe et al., 2021), and deep slow earthquakes in southwest Japan (Ide & Yabe,
839 2014), Cascadia (Ide, 2016), and Mexico (Ide & Maury, 2018). We note that scaled energies of
840 shallow slow earthquakes were estimated for individual events, whereas those of deep slow
841 earthquakes were estimated for stacked events.

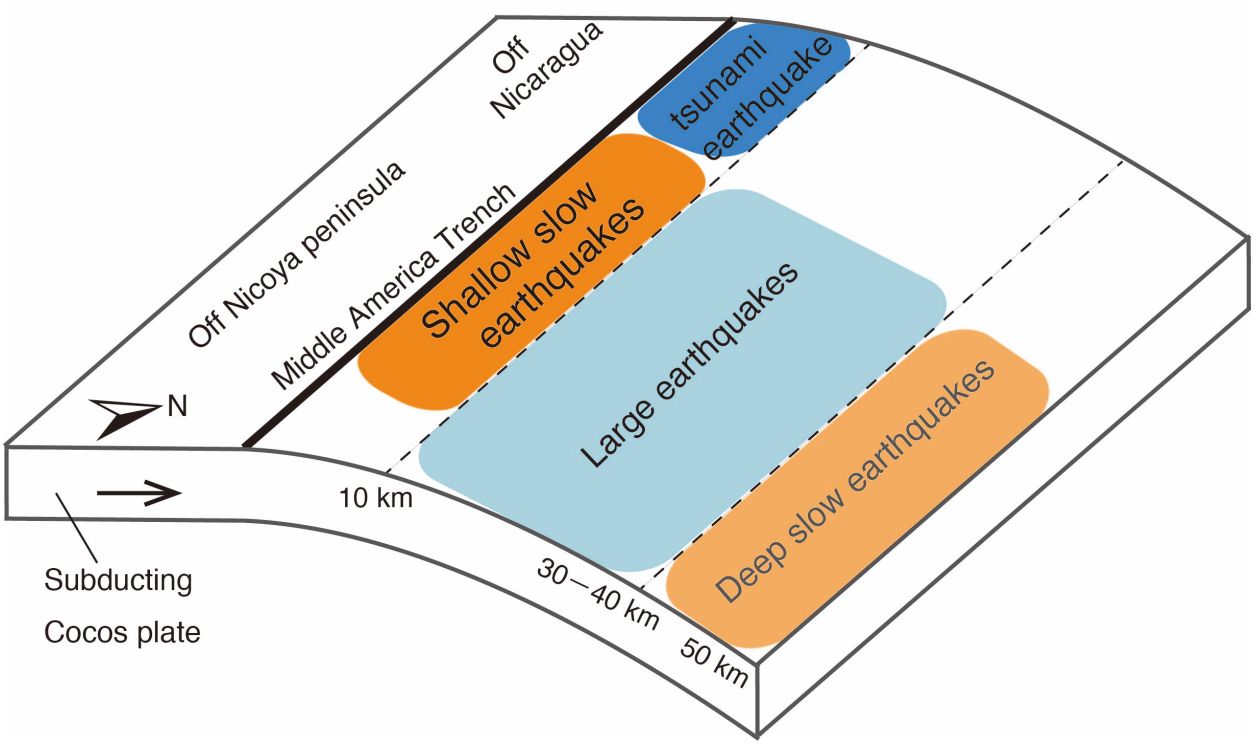

Figure 10. A schematic illustration showing the interpretation of distributions of slow, tsunami, and large regular earthquakes in the Central American subduction zone. The areas of large earthquakes, the 1992 tsunami earthquake, and deep slow earthquakes are referred from Yue et al. (2013), Satake (1994), and Outerbridge et al. (2010), respectively.